Effects of fluctuation in air hole radii and positions on optical characteristics in photonic crystal heterostructure nanocavities

Hiroyuki Hagino, Yasushi Takahashi,* Yoshinori Tanaka, Takashi Asano, and Susumu Noda
Department of Electronic Science and Engineering and Photonics and Electronics Science and Engineering Center, Kyoto University, Kyoto 615-8510, Japan
(Received 17 November 2008; published 17 February 2009)

We investigate the influence of the nanometer-scale variations in the radii and positions of air holes on the optical characteristics for photonic crystal heterostructure nanocavities. The change in the quality factor, the resonant wavelength, the near-field image, and the polarization property are examined using three-dimensional finite difference time domain calculation with random fluctuation patterns. The variations with a standard deviation as small as 1 nm have a clear effect on these optical characteristics, whose magnitudes are strongly dependent on the fluctuation patterns. To prevent this deterioration, the accuracy of the 50 air holes nearest to the nanocavity is the most important.

DOI: 10.1103/PhysRevB.79.085112 PACS number(s): 42.70.Qs, 02.60.Cb, 42.55.Sa, 42.60.Da

I. INTRODUCTION

Nanocavities in two-dimensional (2D) photonic crystal (PC) slabs have attracted much attention in various fields because of their high-quality (Q) factors and small modal volumes.[1–4] Increasing the Q factor of nanocavities is important for advancing the performance of various applications, such as highly sensitive environmental sensors,[5,6] ultrasmall wavelength filters,[7,8] compact optical-buffer memory,[9,10] and quantum-information processing.[11,12] In 2003, we reported an important design rule to increase the Q factor of nanocavities; the form of the cavity electric-field distribution should slowly vary in order to suppress out-of-slab photon leakage.[1] In 2005, we proposed heterostructure nanocavities which enabled the control of the cavity electric-field distribution to an unprecedented extent, where the design Q factor (Q_{ideal}) in calculation exceeded ten million.[2] Shortly thereafter, we fabricated the nanocavities with Q_{ideal} of 15 million and attained an experimental Q factor (Q_{exp}) of approximately one million.[13] We have analytically demonstrated that the lower Q_{exp} can be attributed to various structural imperfections in the fabricated cavities,[14] which give rise to an additional Q factor (Q_{loss}). Since then we have improved the entire fabrication process and in 2007 we succeeded in fabricating the silicon nanocavity with a Q_{exp} of 2.5×10^6, the highest reported so far in PC cavities.[3] However, there is still a large discrepancy between Q_{ideal} and Q_{exp} due to the persisting Q_{loss}.

In line with the developments in high-Q nanocavity research described above, we suspect the main origins of Q_{loss} in our current samples to be nanometer-scale variations in the radii and positions of the air holes composing the nanocavity, which would be inevitable due to the technical limits of the semiconductor process. Because 2D-PC devices operate on the basis of the periodic refractive index change by the air holes, these two types of imperfections can have significant effect on various optical properties for the nanocavities. The reduction in Q by these imperfections was estimated in our previous analyses based on a simple model which assumes that the effect of each air hole imperfection has an independent effect on the Q_{loss}.[14] In fact there must be interactions between imperfections of air holes and thus, more accurate estimation using realistic fluctuation patterns based on three-dimensional (3D) finite difference time domain (FDTD) calculation was required. We used some such calculation results in Ref. 3, however the details of the numerical analysis, the mechanism for the reduction of Q, and the effects on other optical properties were not reported.

In this paper, we report on the influence of the nanometer-scale variations in the air holes' radii and positions on optical characteristics for high-Q nanocavity with a two-step heterostructure. We performed 3D FDTD calculations for the heterostructure nanocavity in which the radii and positions of all air holes were independently varied at random, such that the probability of the variations followed a normal distribution. The reduction in the Q factor, the shift of the resonant wavelength, the change in the near-field image, and the deviation of the polarization properties induced by the variations are investigated using 26 fluctuation patterns. The variations with a standard deviation of as little as 1 nm produce visible deterioration, whose magnitude is strongly dependent on the fluctuation patterns. From calculations where the region of the air holes with variations is restricted, we determine that the accuracy of the 50 air holes nearest to the nanocavity is the most significant for preventing the deterioration.

II. CALCULATION METHOD

Figure 1(a) shows the schematic of the nanocavity structure studied in this work. This nanocavity is based on a 2D PC slab with a triangular lattice of circular air holes and a line-defect waveguide formed by a row of missing air holes. The structural parameters used in the calculation are as follows: the slab thickness is 250 nm, the air holes' radii (r) are 115 nm, the main lattice constant (a_1) is 410 nm, and the refractive index is 3.4 for the slab (silicon). The lattice constant in the x direction increases by 5 nm every two periods as it approaches the center of the cavity to form heterostructure nanocavity, while the lattice constant in the y direction is the same in all regions. This type of nanocavity can realize gradual optical confinement by utilizing the mode gap differences and therefore, the value of Q_{ideal} for this nanocavity

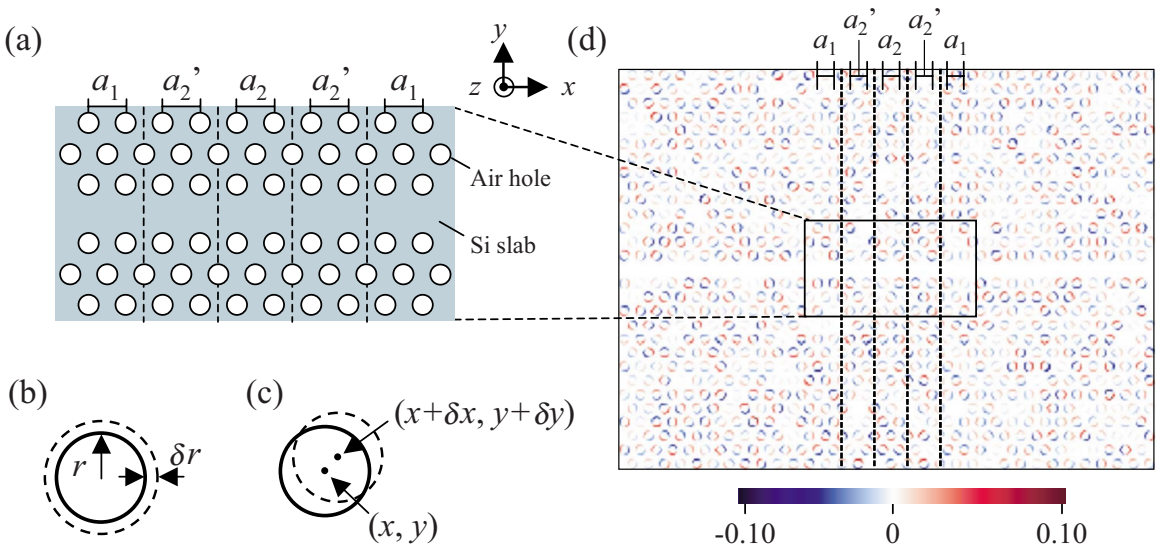

FIG. 1. (Color online) (a) Schematic of the nanocavity with a two-step heterostructure. The lattice constants a_1, a_2', and a_2 are 410, 415, and 420 nm, respectively. The slab thickness and air holes' radii are 250 and 115 nm. (b), (c) Schematic view of the variation in an air hole's radius and in an air hole's position. δr, δx, and δy represent the variations. (d) The difference of the dielectric constant from the ideal structure in a fluctuation pattern for the air holes' position with $\sigma=1$ nm. The dielectric constants of the slab and air are normalized as 1 and 0.

can exceed ten million while still maintaining a small modal volume.[2] However in actuality, the air holes' radii and positions in the fabricated nanocavities must vary from the original design in the nanometer scale. Its influence on the optical characteristics can be examined by 3D FDTD calculation including these variations.

Figures 1(b) and 1(c) clearly illustrate the two variations considered here; the ideal values of the air hole's radius and position are represented by r and (x,y), while the corresponding variations are denoted by δr, and $(\delta x, \delta y)$ (variation in the slab thickness δz is not considered here). We assume that these three variations are introduced at random to all air holes in the fabricated samples, such that the probability of each variation follows a normal distribution with a standard deviation (σ). Such variations were brought into the structure for 3D FDTD using the Mersenne Twister method[15] and the Box Muller method.[16] The former creates the random real numbers between 0 and 1, and the latter converts them into the numbers which fulfill the normal distribution with an arbitrary σ (nanometers). Correlation within and between the fluctuation patterns can be ignored due to the good quality of the random number sequences created by the Mersenne Twister method. In addition, we can independently change the magnitudes of variations for the same fluctuation pattern by changing σ in the latter process.

The sizes of a unit cell in 3D FDTD algorithm are set as 42 nm in the x direction, 45.5 nm in y, and 42 nm in z, respectively. These lengths are about one-tenth of the lattice constant, which means that the electromagnetic waves with a wave number (k) greater than $10\times(2\pi/a)$ are excluded from the calculation. The main components of the nanocavity electromagnetic field are located below $k=2\pi/a$ as will be shown in Fig. 4 so this cutoff is sufficiently high. The dielectric constant (ε) of each FDTD cell is determined by the over-sampling method: first, the distribution of ε for the structure is prepared for microcells whose lengths are 1/20 of the FDTD cell in each direction. Next, the ε of each FDTD cell is determined by averaging the values of the microcells within the FDTD cell. In this method, subnanometer variations in air holes are properly reflected in the distribution of ε used in the calculation within the limit of the cutoff wave number described above. Figure 1(d) shows an example of the difference of the dielectric constant between the ideal structure and a fluctuation pattern where only the air holes' positions are randomly varied with $\sigma=1$ nm. The cells where the ε increases and decreases are colored . It is apparent that even with $\sigma=1$ nm, the variations are reflected into the calculation.

The total calculation area is set as $48a_2$ in the x direction, $35a_2$ in y, and $13a_2$ in z, respectively. The nanocavity shown in Fig. 1(a) is located at the center of the area. The region where air holes are varied is $32a_2$ in the x direction and $24a_2$ in y as shown in Fig. 1(d). The perfectly matched layer (PML) is located at the edge of calculation area, which absorbs light leaving the calculated region without the reflection. The distance from the nanocavity to the edge of PML is $19a_2$ in the x direction, $15a_2$ in y, and $4.5a_2$ in z, respectively. We confirmed that the PML was sufficiently far from the cavity so that the PML did not affect the nanocavity mode. We excited the nanocavity mode by a Gaussian pulse of the magnetic field in the z direction (H_z) with pulse width of $0.0005\times(c/a_2)$. The time period of calculation step is 0.07 fs ($a_2/20c$). The total calculation steps are 80 000 ($4000a_2/c$), which is long enough to avoid the influence of the excitation pulse. We calculated the Q factor for the nanocavity from the time decay of the pointing vector passing through an observation plane surrounding the cavity and the resonant wavelength of the nanocavity was calculated by Fourier transform of the time change in H_z at the center of the cavity. In the case of $\delta r=\delta x=\delta y=0$, the Q factor (Q_{ideal})

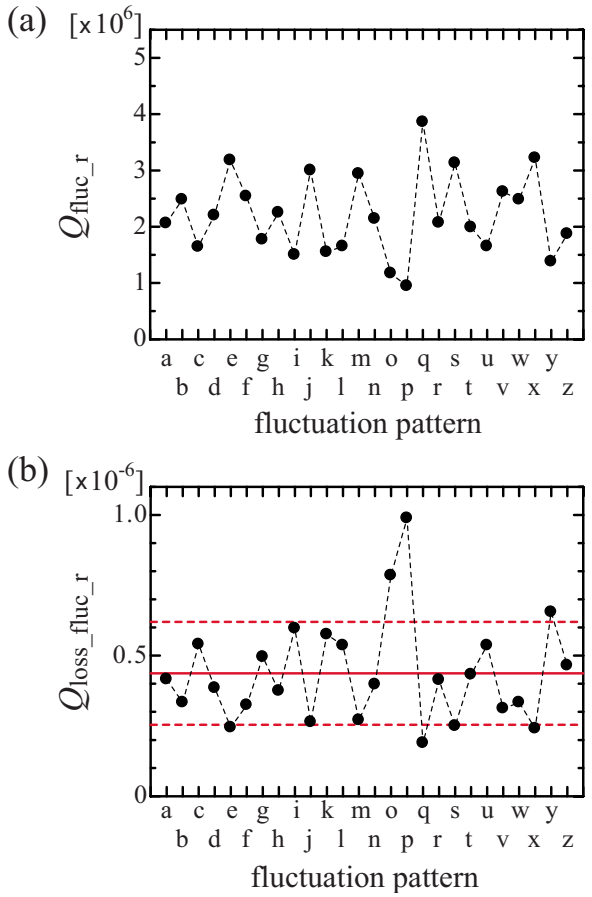

FIG. 2. (Color online) (a) The Q factors of the nanocavity for 26 fluctuation patterns $a-z$, in which air holes' radii are varied with $\sigma=1$ nm. (b) The optical losses due to the variation of air hole radius for 26 patterns. The solid (dashed) line indicates the average of losses (the average $\pm\Sigma$).

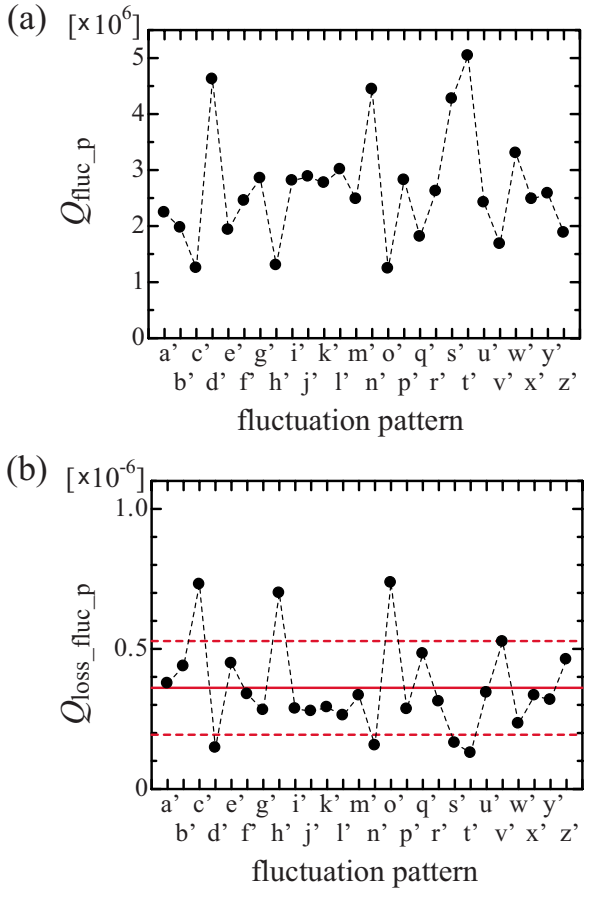

FIG. 3. (Color online) (a) The Q factors for 26 fluctuation patterns $a'-z'$, in which air holes' positions are varied with $\sigma=1$ nm. (b) The optical losses due to the variation in air hole position for 26 patterns. The solid (dashed) line indicates the average of losses (the average $\pm\Sigma$).

is calculated to be 1.5×10^7 and the resonant wavelength is 1589.28 nm.

We carried out the calculation in three fluctuation cases: only variation in hole radius δr, only variation in hole position $(\delta x, \delta y)$, and with both variations. Based on the accuracy of our current fabrication process, the target value of σ was set between 0.5 and 3.5 nm. Because the value of Q depends on the fluctuation patterns, we performed the calculation for three fluctuation cases with 26 different fluctuation patterns each.

III. CALCULATION RESULTS AND DISCUSSION

A. Cases with either the air holes' radii or positions varied with $\sigma=1$ nm

Figure 2(a) presents the calculated Q factors ($Q_{\text{fluc\_r}}$) of the nanocavity for different 26 fluctuation patterns denoted by $a-z$, in which the air holes' radii are randomly varied with $\sigma=1$ nm. It is obvious that $Q_{\text{fluc\_r}}$ all decrease significantly from the Q_{ideal} of 1.5×10^7 and are strongly dependent on the fluctuation patterns. We can define an additional Q factor due to the fluctuation of air holes' radii as $Q_{\text{loss\_fluc\_r}}$ where the relationship is given by

$$\frac{1}{Q_{\text{fluc\_r}}}=\frac{1}{Q_{\text{ideal}}}+\frac{1}{Q_{\text{loss\_fluc\_r}}}. \tag{1}$$

Figure 2(b) displays the corresponding $1/Q_{\text{loss\_fluc\_r}}$ for 26 patterns. The $1/Q_{\text{loss\_fluc\_r}}$ indicates the optical loss of the nanocavity due to the fluctuation of air holes' radii. The average of $1/Q_{\text{loss\_fluc\_r}}$ is 4.37×10^{-7} (solid line) and the standard deviation (Σ) is 1.83×10^{-7} (dashed lines). It is noted that the standard error of 3.36×10^{-8} arises from the finite number of the fluctuation patterns. In this paper, we define the Q factor determined from the Q_{ideal} and the average of $1/Q_{\text{loss\_fluc\_r}}$ as the expectation value of $Q_{\text{fluc\_r}}$. Then, the expectation value of $Q_{\text{fluc\_r}}$ with the air holes' variation of $\sigma=1$ nm is evaluated to be 1.99×10^6. The minimum and maximum $Q_{\text{fluc\_r}}$ within the Σ are 1.46×10^6 and 3.12×10^6, respectively.

Figure 3(a) shows the $Q_{\text{fluc\_p}}$ for 26 fluctuation patterns $a'-z'$, in which air holes' positions are randomly varied with $\sigma=1$ nm. These fluctuation patterns are different from those used in Fig. 2. The $Q_{\text{fluc\_p}}$ are also reduced significantly and are also strongly dependent on the fluctuation patterns. We similarly define an additional Q factor due to the variation of

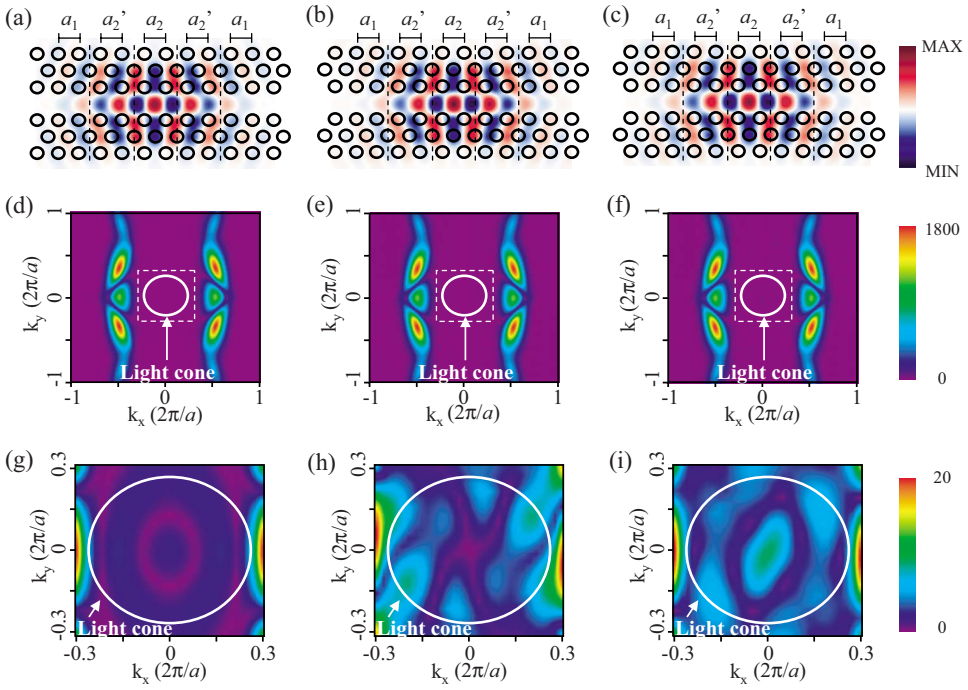

FIG. 4. (Color online) Comparison of the nanocavity modes for three cases. The left column is to the case of no fluctuation. The middle column corresponds to the variation in radius in fluctuation pattern z in Fig. 2. The right column corresponds to the variation of position in fluctuation pattern z' in Fig. 3. [(a)–(c)] The electric-field distributions of E_y for the nanocavity modes. [(d)–(f)] The Fourier transform of E_y. The white circles represent the light cone. [(g)–(i)] The magnified views around the light cone.

air holes' positions as $Q_{\text{loss\_fluc\_p}}$ where the relationship is given by

$$\frac{1}{Q_{\text{fluc\_p}}} = \frac{1}{Q_{\text{ideal}}} + \frac{1}{Q_{\text{loss\_fluc\_p}}}. \tag{2}$$

Figure 3(b) shows the $1/Q_{\text{loss\_fluc\_p}}$ for the 26 patterns, in which the average of $1/Q_{\text{loss\_fluc\_p}}$ is 3.61×10^{-7} and the Σ is 1.67×10^{-7}. These values are comparable with those estimated in Fig. 2(b). The expectation value of $Q_{\text{fluc\_p}}$ is 2.34×10^{6}, and the minimum and maximum $Q_{\text{fluc\_r}}$ within the Σ are 1.68×10^{6} and 3.84×10^{6}, respectively.

The electric-field distributions of nanocavity modes with and without variations are compared in Fig. 4, where the left column corresponds to the ideal structure ($\sigma=0$ nm), the middle column corresponds to the fluctuation pattern z used in Fig. 2 ($\sigma=1$ nm), and the right column corresponds to the fluctuation pattern z' used in Fig. 3 ($\sigma=1$ nm). Figures 4(a)–4(c) show the normalized electric-field distributions of y component, E_y, on the slab surface at the end of the calculation, that represent the nanocavity modes. Figures 4(d)–4(f) are the absolute value of the spatial Fourier transform of E_y in Figs. 4(a)–4(c), where the white circles represent the light cone which denotes the boundary in k space at side of which the total reflection condition between the slab and the air is satisfied. The quantity of component in the light cone defines the Q factor of the nanocavity. Figures 4(g)–4(i) are the magnified views around the light cone denoted by the dashed line in Figs. 4(d)–4(f). We can see that the electric-field distribution and the main components in k space for the nanocavity mode are hardly deformed by the nanometer-scale variations. However, it is also clear that the components within the light cone increase due to the variations. This increase could be interpreted as the scattering of the original components into the light cone due to the variations. The probability for scattering into the light cone could strongly depends on the fluctuation pattern, and thus, the Q factors naturally change randomly as shown in Figs. 2(a) and 3(a). It is clearly demonstrated in Figs. 2–4 that both variations in air holes' radii and positions significantly reduce the Q factor of the heterostructure nanocavity even when the σ is as small as 1 nm.

B. Cases when the air holes' radii and positions are varied simultaneously with $\sigma=1$ nm

Figure 5(a) shows the $1/Q_{\text{loss\_fluc\_r+p}}$ for 26 fluctuation patterns $A-Z$ where both the air holes' radii and positions are varied simultaneously with $\sigma=1$ nm. The patterns $A-Z$ are the sum of the patterns used in Figs. 2 and 3; $A=a+a'$, $Z=z+z'$. The average of $1/Q_{\text{loss\_fluc\_r+p}}$ is 7.61×10^{-7} and the Σ is 3.57×10^{-7}. These values are close to the sum of those estimated in Figs. 2(b) and 3(b). The expectation of $Q_{\text{fluc\_r+p}}$ is estimated to be 1.21×10^{6} and the minimum and maximum $Q_{\text{fluc\_r+p}}$ within the Σ are 8.44×10^{5} and 2.12×10^{6} from the relation,

$$\frac{1}{Q_{\text{fluc\_r+p}}} = \frac{1}{Q_{\text{ideal}}} + \frac{1}{Q_{\text{loss\_fluc\_r+p}}}. \tag{3}$$

The influence of the variations on the resonant wavelengths, the near-field images, and the polarization properties for the nanocavity are also investigated for the 26 patterns $A-Z$. Figure 5(b) shows the resonant wavelengths for $A-Z$. The resonant wavelength also fluctuate, however, there seems to be no correlation to the reduction in $Q_{\text{fluc\_r+p}}$. This is because the shift of the resonant wavelength is derived from the change in the refractive index relative to the cavity mode field distribution, which is different from the cause of the reduction of $Q_{\text{fluc\_r+p}}$ discussed in Fig. 4. The average of the resonant wavelengths is 1589.21 nm and the Σ is 0.73 nm. The average value is close to the wavelength of 1589.28 nm for the ideal structure.

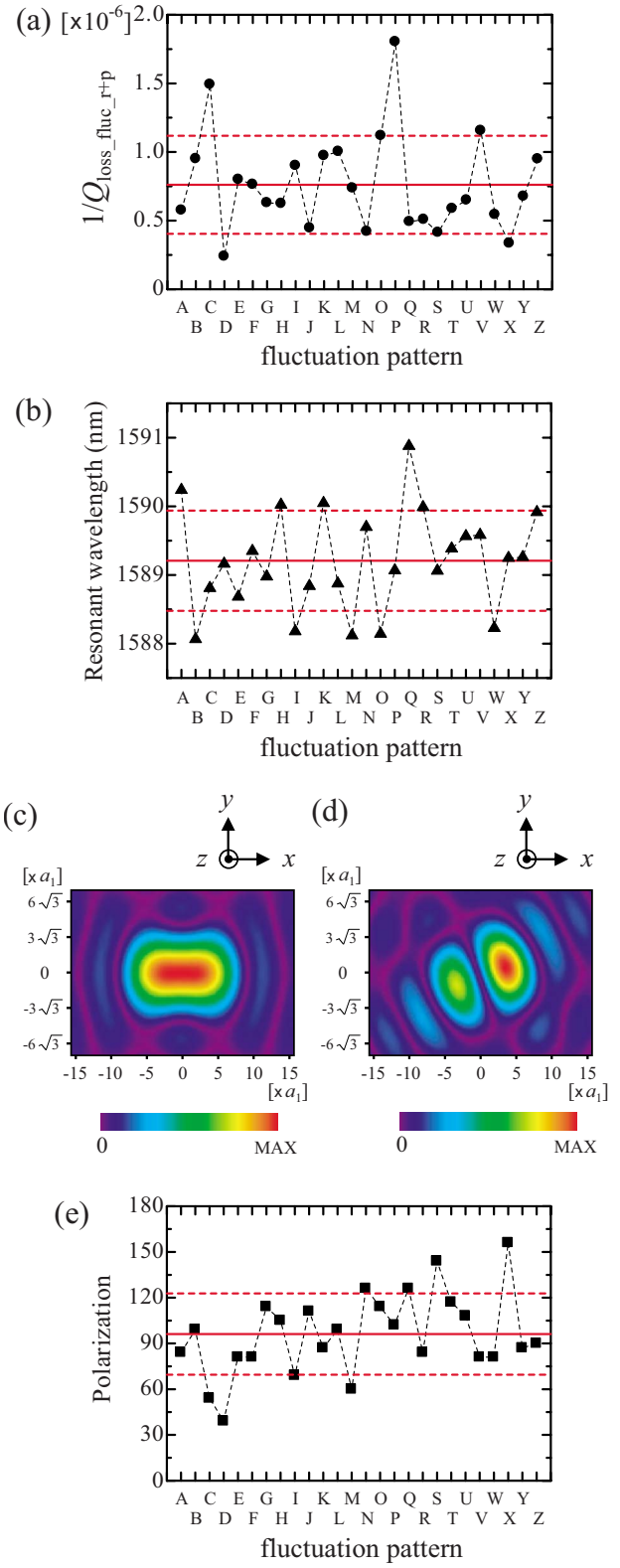

FIG. 5. (Color online) The optical characteristics of nanocavities where the air holes' radii and positions fluctuate simultaneously with $\sigma=1$ nm. (a) The optical losses for the 26 fluctuation patterns $A-Z$. The solid (dashed) line indicates the average (average $\pm\Sigma$). (b) The resonant wavelengths for the 26 patterns. (c) The near-field image without fluctuations. (d) Image for representative fluctuation pattern H. (e) The polarizations of the near-field images for the 26 patterns.

Figures 5(c) and 5(d) show the near-field images of the radiation from the nanocavity, assuming observation via an objective lens with numerical aperture of 0.4. Figures 5(c) and 5(d) correspond to the cases without the fluctuations and with the fluctuation pattern H, respectively. The ideal structure has a single lobed spot while certain fluctuation patterns create the multiple lobes, as in the example shown in Fig. 5(d). About 60% of the 26 patterns had single lobed spots.

Figure 5(e) shows the polarization angles, at which the transmittance through a linear polarizer is maximum, in the images for 26 patterns. 0° corresponds to the x direction and the polarization angle for Fig. 5(c) is 90°. It is shown that the polarization angle also fluctuates, where the average angle is 96.1° and the Σ is 26.6°. Though not shown here, the polarization linearity also fluctuates. The details of the analysis method for spatial patterns and polarization properties in PC nanocavities have been reported previously.[17,18]

It is noted that the expectation of $Q_{\text{fluc\_r+p}}$ and the maximum $Q_{\text{fluc\_r+p}}$ within the Σ estimated from Fig. 5(a) correspond closely to recent experimental results of nanocavities with a two-step heterostructure.[3] Furthermore, the random fluctuations of optical characteristics agree with the experimental results for the nanocavities. The fluctuations of the Q_{exp} and the resonant wavelengths among the nanocavities fabricated on the same chip have been reported in Ref. 3. The random deteriorations of emission pattern and polarization linearity have been reported in Ref. 19. Therefore, both variations in radius and position on the order of 1 nm certainly exist in current fabricated samples[20] and are essential components of Q_{loss}.

It is important to consider the effect of the nanometer-scale variations on other nanocavity designs. If the order of the $1/Q_{\text{loss\_fluc\_r+p}}$ does not change in other nanocavities, the influence is negligible for nanocavities with lower Q_{ideal}, such as the L3 cavity ($Q_{\text{ideal}}=5000$).[1] Conversely, they could be significant for high-Q nanocavities utilizing mode gap confinement.[21–24] Similar consideration would be applicable for the characteristics of emission patterns and polarization angles. In contrast, the shift of the resonant wavelength due to these variations would occur equally in high-Q and lower-Q nanocavities.[25]

C. Cases with different standard deviations of the variations

Figure 6(a) shows the dependence of optical loss ($1/Q_{\text{loss\_fluc\_r+p}}$) on the magnitude of the variations (σ). The symbols in Fig. 6(a) show the values calculated by 3D FDTD for the various σ of 0.5, 1.0, 2.0, and 3.0 nm, where the fluctuation patterns $A-E$ are selected as examples. The $1/Q_{\text{loss\_fluc\_r+p}}$ reasonably increases for all patterns with increase in σ, which corresponds to the increase in the components within the light cone shown in Fig. 4. The dashed lines in Fig. 6(a) represent the fittings by using the quadratic functions given by

$$\frac{1}{Q_{\text{loss\_fluc\_r+p}}} = A_m \sigma^2, \tag{4}$$

where m denotes the fluctuation patterns and A_m is the coefficient for each pattern. The fittings are in good agreement

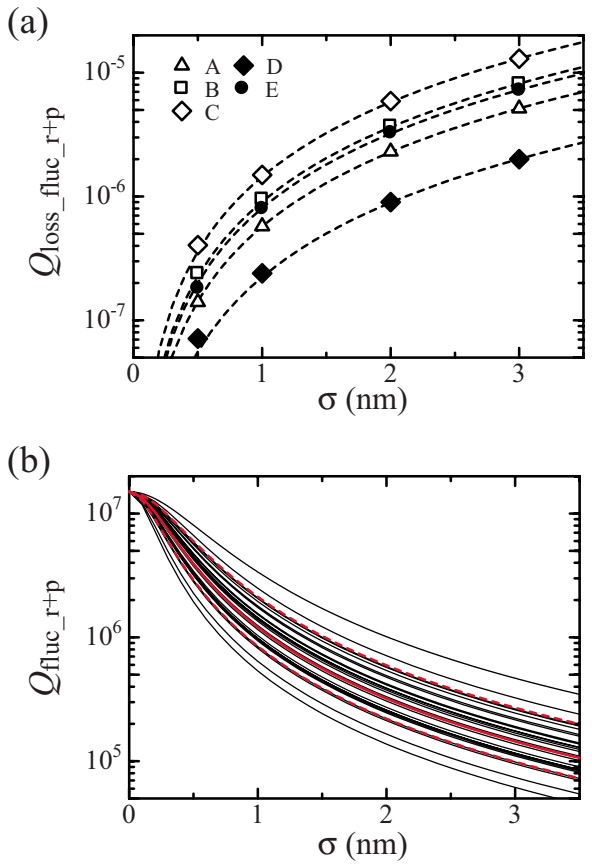

FIG. 6. (Color online) (a) Dependence of the optical loss on σ. The symbols indicate the calculation results for σ of 0.5, 1.0, 2.0, and 3.0 nm in the fluctuation patterns $A-E$. The dashed lines represent fittings. (b) Approximate dependence of the $Q_{\text{fluc\_r+p}}$ on σ in the 26 patterns $A-Z$. The solid (dashed) line indicates the average (the average $\pm\Sigma$). The value at $\sigma=0$ nm is 15 million.

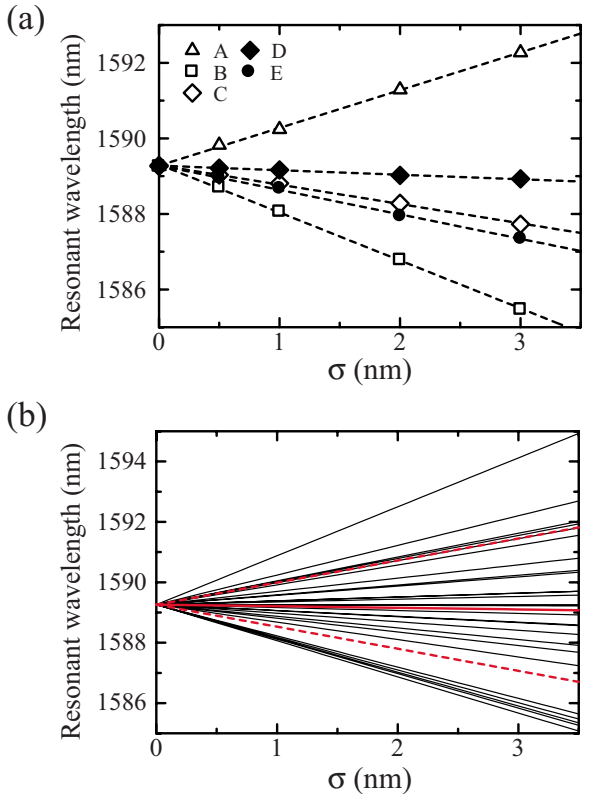

FIG. 7. (Color online) (a) Dependence of the resonant wavelength on σ. The symbols indicate the calculation results for σ of 0.5, 1.0, 2.0, and 3.0 nm in the fluctuation patterns $A-E$. The dashed lines represent the fittings. (b) The approximate dependence of the resonant wavelength on σ in the 26 patterns $A-Z$. The solid (dashed) line indicates the average (the average $\pm\Sigma$). The value at $\sigma=0$ nm is 1589.28 nm.

with the calculated data for all patterns. This agreement can be explained theoretically as follows. In the calculation model of Figs. 1(b) and 1(c), the dielectric-constant change ($\Delta\varepsilon$) due to the variations are proportional to σ ($\Delta\varepsilon \propto \sigma$) for both cases. It is well known that the optical scattering loss for the waveguide is proportional to the square of the $\Delta\varepsilon$ ($1/Q_{\text{loss}} \propto \Delta\varepsilon^2$).[26,27] Since this mechanism could be applied to the nanocavity, $1/Q_{\text{loss\_fluc\_r+p}}$ is proportional to the σ^2. By substituting Eq. (4) into Eq. (3), $Q_{\text{fluc\_r+p}}$ for a certain fluctuation pattern is obtained as a function of σ as follows:

$$Q_{\text{fluc\_r+p}} = \frac{1}{1/Q_{\text{ideal}} + A_m\sigma^2}. \tag{5}$$

Because we can determine the A_m for the data shown in Fig. 5(a) by applying Eq. (4), the dependences of $Q_{\text{fluc\_r+p}}$ on the σ can be obtained for the 26 patterns without carrying out the simulation for individual σ.

Figure 6(b) shows the dependence of the $Q_{\text{fluc\_r+p}}$ on the σ in the 26 fluctuation patterns $A-Z$ using Eq. (5). The red solid line indicates the expectation of $Q_{\text{fluc\_r+p}}$ where the corresponding value of A_m is 7.61×10^{-7}. The red dashed lines represent the standard deviation (Σ) where the corresponding A_m are 4.04×10^{-7} and 1.12×10^{-6}. These data suggest the prospect of enhancing the Q_{exp} factor by the progress of process techniques. If we can fabricate nanocavities with air holes variations in $\sigma=0.5$ nm (0.3 nm), the average of the Q_{exp} will rise to about 3.9×10^6 (7.4×10^6) and Q_{exp} greater than 6.0×10^6 (1.0×10^7) will be obtained with a probability of 10% from a normal distribution.

Figure 7(a) shows the resonant wavelengths for the various σ in fluctuation patterns $A-E$. The resonant wavelength shift from 1589.28 nm ($\sigma=0$ nm) is proportional to the increase of σ. It is well known that the shift of the resonant wavelength is linear over the deviation of the refractive index averaged in the cavity mode field,[28] which increases in proportion to the σ in our model. The dashed lines represent the fittings using the following linear function:

$$\lambda = B_m\sigma + 1589.28, \tag{6}$$

where λ is the resonant wavelength in nanometers and B_m is the coefficient for each fluctuation pattern. The fitting results are in good agreement with the calculated results. We can obtain B_m for the data shown in Fig. 5(b) and therefore, the dependencies of the resonant wavelength on σ are obtained for the 26 patterns shown in Fig. 7(b). The red solid line indicates the average of the resonant wavelengths and the red dashed lines represent the Σ. The average values are in good

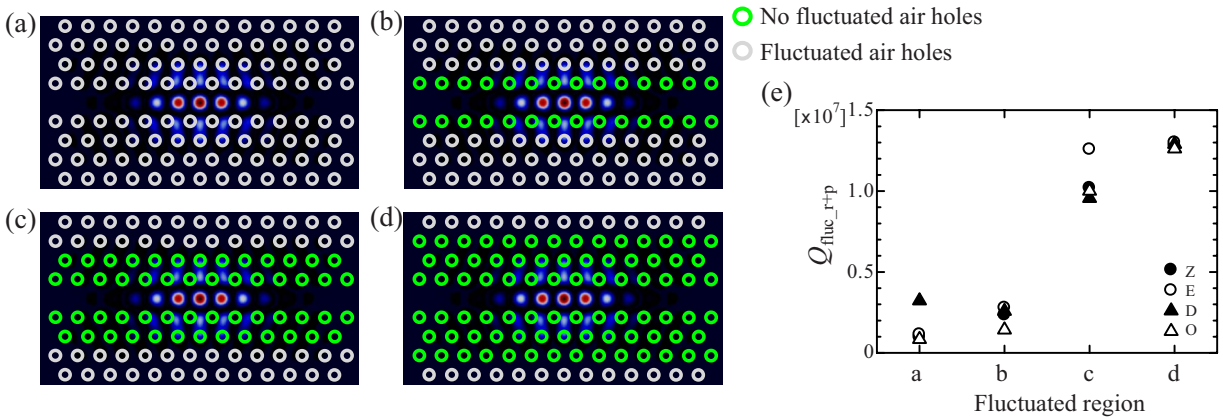

FIG. 8. (Color online) [(a)–(d)] Calculation models in which the colored air holes are not varied (σ=0 nm) while the white air holes fluctuate in both position and radius with σ=1 nm. The superimposed images are the squared electric-field distribution $|E_y|^2$. (e) Calculated Q factors for the fluctuation cases of (a)–(d). The four fluctuation patterns in Fig. 5(a) are used in calculation.

agreement with the original wavelength of 1589.28 nm. Because the fluctuation of the resonant wavelength of the nanocavity is a problem for various applications, research into nanocavities with resonant wavelengths that are resistant to these fluctuations will be needed.

If we experimentally investigate the Q factors and the resonant wavelengths for many nanocavities with the same structure, we could estimate the magnitude of the variations in the fabricated samples from the comparison with Figs. 6(b) and 7(b). This estimation will be important because the subnanometer variations in the air holes for the fabricated samples cannot be evaluated directly by conventional observation methods (scanning electron microscopy, atomic force microscopy, optical microscopy, etc.). If the value of σ evaluated from the average of Q_{exp} was larger than that evaluated from the Σ of the resonant wavelengths, it would suggest that other factors are contributing to Q_{loss}, such as water on the sample surface[14] or surface states.[29]

D. Cases when the air holes around the nanocavity are not varied

Finally, we investigate which air holes are most responsible for the reduction in Q factor when they fluctuate. Such information would be useful for reducing the total time of electron-beam lithography and for designing novel nanocavity structures that are resistant to the variations. Figures 8(a)–8(d) show the calculation models in which the colored air holes are not varied while the white holes fluctuate in both position and radius with σ=1 nm. The images superimposed on the figures indicate the squared electric-field distribution of $|E_y|^2$. All air holes fluctuate at random in Fig. 8(a) and two, four, and six rows of air holes next to the line defect are left unvaried in Figs. 8(b)–8(d), respectively. The four fluctuation patterns are used in calculating patterns, D, E, O, and Z. The pattern D (O) corresponds to the case of the lowest (highest) $1/Q_{\mathrm{loss\_fluc\_r+p}}$ in Fig. 5(a). Figure 8(e) presents the calculated results for each fluctuation case. The

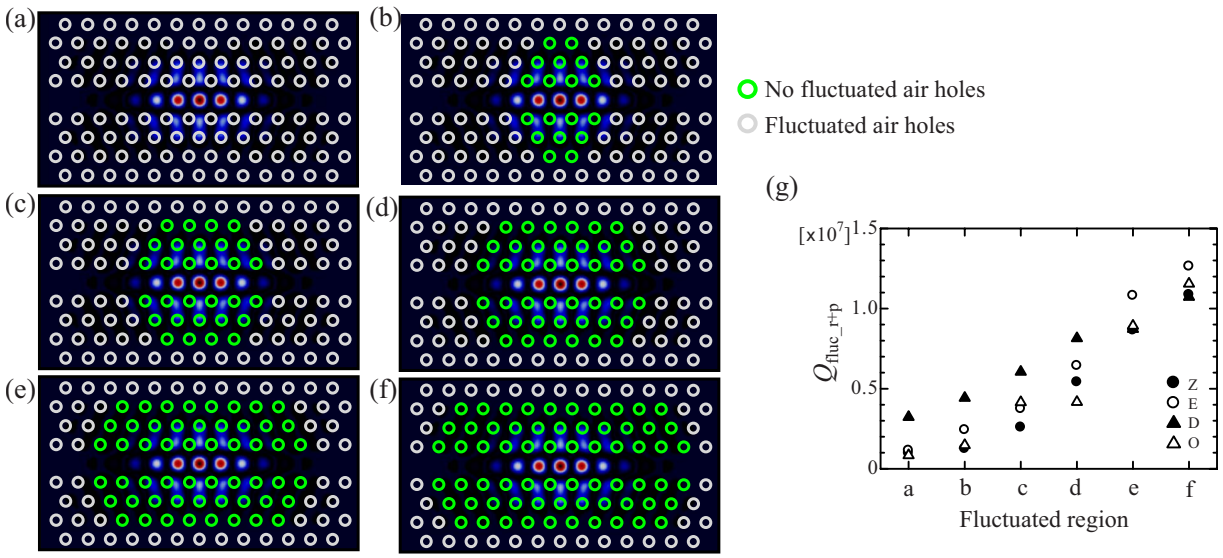

FIG. 9. (Color online) [(a)–(f)] Calculation models in which the colored air holes are not varied (σ=0 nm) while the white air holes fluctuate with σ=1 nm. The superimposed images are $|E_y|^2$. (g) Calculated Q factors for the fluctuation cases of (a)–(f). The four fluctuation patterns in Fig. 5(a) are used in calculation.

average of $Q_{\text{fluc\_r+p}}$ abruptly increases in the case of Fig. 8(c) and $Q_{\text{fluc\_r+p}}$ exceeds 10 million for all patterns in the case of Fig. 8(d).

Figure 9 shows the calculation when the number of the air holes with no variations increase in the x direction. Figures 9(a)–9(f) show the calculation models. The same fluctuation patterns as Fig. 8 are used in this calculation. Figure 9(g) presents the calculated results for each fluctuation case. The $Q_{\text{fluc\_r+p}}$ gradually increases with broadening of the region where air holes have no variations and $Q_{\text{fluc\_r+p}}$ exceeds ten million for all patterns in case Fig. 9(f). In Fig. 9(f), 99% of the nanocavity mode energy is contained in the region with ideal air holes. It is clear from these calculations that the variations in air holes nearest to the nanocavity are the most significant in the reduction in Q. We confirmed that similar relationships were obtained for the resonant wavelength, the near-field image, and the polarization.

IV. SUMMARY

We have numerically investigated the influence of random nanometer-scale variations of air holes' radii and positions on the optical characteristics of 2D PC nanocavities with Q_{ideal} of 1.5×10^7. The reduction in Q factor, the shift of the resonant wavelength, the change in the near-field image, and the deviation of the polarization properties are brought about by variations of as little as 1 nm. The magnitude of the deterioration is strongly dependent on the fluctuation patterns. From calculations where the region of the air holes with the variations is restricted, we determine that the accuracy of the 50 air holes nearest to the nanocavity is the most significant for preventing this deterioration and for achieving higher-Q_{exp} factors.

ACKNOWLEDGMENTS

This work was partly supported by the Core Research for Evolutional Science and Technology of the Japan Science and Technology Agency, by the Global COE Program, by Special Coordination Funds for Promoting Science and Technology and Research Grants, and by a Grant-in-Aid from the Ministry of Education, Culture, Sports, Science and Technology-Japan.

*ytakahashi@qoe.kuee.kyoto-u.ac.jp

[1] Y. Akahane, T. Asano, B. S. Song, and S. Noda, Nature (London) **425**, 944 (2003).
[2] B. S. Song, S. Noda, T. Asano, and Y. Akahane, Nature Mater. **4**, 207 (2005).
[3] Y. Takahashi, H. Hagino, Y. Tanaka, B. S. Song, T. Asano, and S. Noda, Opt. Express **15**, 17206 (2007).
[4] S. Noda, M. Fujita, and T. Asano, Nat. Photonics **1**, 449 (2007).
[5] M. Lee and P. M. Fauchet, Opt. Express **15**, 4530 (2007).
[6] S. Kita, K. Nozaki, and T. Baba, Opt. Express **16**, 8174 (2008).
[7] H. Takano, B. S. Song, T. Asano, and S. Noda, Opt. Express **14**, 3491 (2006).
[8] B. S. Song, T. Nagashima, T. Asano, and S. Noda, IEEE Photon. Technol. Lett. **20**, 532 (2008).
[9] Y. Tanaka, J. Upham, T. Nagashima, T. Sugiya, T. Asano, and S. Noda, Nature Mater. **6**, 862 (2007).
[10] J. Upham, Y. Tanaka, T. Asano, and S. Noda, Opt. Express **16**, 21721 (2008).
[11] T. Yoshie, A. Scherer, J. Hendrickson, G. Khitrova, H. M. Gibbs, G. Rupper, C. Ell, O. B. Shchekin, and D. G. Deppe, Nature (London) **432**, 200 (2004).
[12] K. Hennessy, A. Badolato, M. Winger, D. Gerace, M. Atature, S. Gulde, S. Falt, E. L. Hu, and A. Imamoglu, Nature (London) **445**, 896 (2007).
[13] T. Asano, B. S. Song, Y. Akahane, and S. Noda, IEEE J. Sel. Top. Quantum Electron. **12**, 1123 (2006).
[14] T. Asano, B. S. Song, and S. Noda, Opt. Express **14**, 1996 (2006).
[15] M. Matsumoto and T. Nishimura, ACM Trans. Model. Comput. Simul. **8**, 3 (1998).
[16] G. E. P. Box and Mervin E. Muller, Ann. Math. Stat. **29**, 610 (1958).
[17] Y. Akahane, M. Mochizuki, T. Asano, Y. Tanaka, and S. Noda, Appl. Phys. Lett. **82**, 1341 (2003).
[18] Y. Akahane, T. Asano, B. S. Song, and S. Noda, Appl. Phys. Lett. **83**, 1512 (2003).
[19] Y. Takahashi, Y. Tanaka, H. Hagino, T. Asano, and S. Noda, Appl. Phys. Lett. **92**, 241910 (2008).
[20] In fabricated samples, the actual surface roughness of the inner walls exceeds 1 nm and the shape of the air holes deviates from perfect circle. We consider these imperfections to be accounted for on average by the variations in the radii and center positions of the air holes.
[21] E. Kuramochi, M. Notomi, S. Mitsugi, A. Shinya, T. Tanabe, and T. Watanabe, Appl. Phys. Lett. **88**, 041112 (2006).
[22] S. Tomljenovic-Hanic, M. J. Steel, C. M. Sterke, and D. J. Moss, Opt. Lett. **32**, 542 (2007).
[23] S. H. Kwon, T. Sunner, M. Kamp, and A. Forchel, Opt. Express **16**, 4605 (2008).
[24] Y. Tanaka, T. Asano, and S. Noda, J. Lightwave Technol. **26**, 1532 (2008).
[25] L. Ramunno and S. Hughes, Conference on Lasers and Electro-Optics/*Quantum Electronics and Laser Science Conference*, QFH7, San Jose, 2008).
[26] D. G. Hall, J. Opt. Soc. Am. A **2**, 747 (1985).
[27] S. Hughes, L. Ramunno, J. F. Young, and J. E. Sipe, Phys. Rev. Lett. **94**, 033903 (2005).
[28] R. A. Waldron, IEEE Trans. Sonics Ultrason. **18**, 16 (1971).
[29] M. Borselli, T. J. Johnson, and O. Painter, Appl. Phys. Lett. **88**, 131114 (2006).